# Dalton Transactions

Accepted Manuscript






ROYAL SOCIETY OF CHEMISTRY

www.rsc.org/dalton

Journal Name

ARTICLE

# Impacts of Terminal Modification of $[Ru(phen)_2dppz]^{2+}$ on the Luminescence Properties: a Theoretical Study

Received 00th January 20xx,
Accepted 00th January 20xx

DOI: 10.1039/x0xx00000x

www.rsc.org/

Xing Gao, Shuo Shi,* Jun-Liang Yao, Juan Zhao, and Tian-Ming Yao.*

$[Ru(phen)_2dppz]^{2+}$ and other closely related ruthenium (II) complexes containing π-extended ligands were found to be non or weakly emissive in water, while had significant luminescence intensity growth when bound to DNA, however, a satisfactory interpretation has not been provided on this "light switch" mechanism. In the present study, we investigated the vertical transitions and triplet excited states of $[Ru(phen)_2dppz]^{2+}$ (**1**), $[Ru(phen)_2dppzi]^{2+}$ (**2**) and $[Ru(phen)_2dppz\text{-}idzo]^{2+}$ (**3**) in gas phase and water solution, through time dependent-density functional theory (TDDFT). Based on the optimized $^3$MLCT and $^3$LLCT structures and energies, we found that the $^3$MLCT state might be responsible for the emissions of the complexes. Interesting connections between the singlet vertical transitions and the luminescence properties were noticed. Through ZORA-TDDFT calculation with SOC perturbatively, we evaluated the intersystem crossing between the lowest singlet excited state, and both $^3$MLCT state and $^3$LLCT state, which gave a reasonable explanation of the luminescence properties of these complexes.

## Introduction

Over the past two decades, ruthenium (II) polypyridine complexes have attracted lots of attention, due to their intriguing photophysical, photochemical, and electrochemical properties, which make them ideal as components in photochemical molecular devices,[1, 2] light-driven catalysis[3] and dye-sensitized solar cells.[4] Ever since the initial report of $[Ru(L)_2dppz]^{2+}$ (L = bpy = 2,2'-bipyridine, L = phen = 1,10-phenanthroline; dppz = dipyrido-[3,2-a:2',3'-c]phenazine) which may serve as remarkable "light-switch" for DNAs, polypyridine ruthenium (II) complexes have gained widely usage in analytical and biological chemistry.[5-9] For instance, $[Ru(L)_2dppz]^{2+}$ were used to sense the mismatch of double-stranded DNA,[10] distinguish the G-quadruplexes architecture form other kind of DNAs,[7, 11] and also detect amyloid-β (Aβ) aggregations in Alzheimer's disease.[12-15]

These usages were all founded on the remarkable "light switch" properties of $[Ru(L)_2dppz]^{2+}$. The luminescence of $[Ru(L)_2dppz]^{2+}$ could hardly be detected when it was dissolved in water, however, the involvement of DNAs, Aβ aggregations or aprotic solvents could greatly promote the strong red luminescence at around 610 nm. To elucidate the "light switch" mechanism of $[Ru(L)_2dppz]^2$ complex, lots of experimental and theoretical studies were carried out.[7,16-22] By using time-resolved emission spectrum of $[Ru(phen)_2(dppz)]^{2+}$ (**1**), Olson demonstrated that when the complex was dissolved in water, another MLCT (metal to ligand charge transfer) state, which lied lower than the MLCT in acetonitrile on energy level, existed and made the excited state relaxation much quicker in a non-luminescence-emission way. This new MLCT (dark state) was mainly localized largely on phenazine (phz) (**Scheme 1**) part of the dppz ligand, while the bright state was associated with the bipyridine (bpy) fragment.[16] Later, Brennaman et al proved that the dark state of $[Ru(bpy)_2(dppz)]^{2+}$ was always the lowest in energy, and they also suggested that the excited-state charge distribution in the bright state was similar in size to that present in the $^3$MLCT state of $[Ru(bpy)_3]^{2+}$.[17]

Researchers who were devoted to quantum computational investigations on the $[Ru(L)_2(dppz)]^{2+}$ complexes have also accomplished lots of achievements. Most of these calculations were based on semiempirical approaches and DFT (density functional theory). By using combined TDDFT (time-dependent density functional theory) calculations and INDO (intermediate neglect of differential overlap) formalism, Pourtois et al pointed out that the dark state in previously proposed models was a low-lying triplet state centered mainly on the π-extended ligands.[18] However, the excitation energies of this work were obtained using different methods, and made the energy results not dependable and comparable. Furthermore, strong luminescence of the three π-extended complexes studied by Pourtois in the presence of DNA, made it hard to identify the calculated bright state. A TDDFT combined self-consistent field (ΔSCF) study showed that, for $[Ru(bpy)_2dppz(H_2O)_2]^{2+}$, the new $^3$MLCT with charge transfer to

[a] Shanghai Key Lab of Chemical Assessment and Sustainability, Department of Chemistry, Tongji University, 1239 Siping Road, 200092,Shanghai, PR China..
† E-mail: shishuo@tongji.edu.cn (S. Shi), tmyao@tongji.edu.cn (T. Yao)
Electronic Supplementary Information (ESI) available: [*Fig. S1-S2, Table S1-S7, coordinates of optimized complexes*]. See DOI: 10.1039/x0xx00000x

the dppz ligand which was the lowest in energy, was the bright state.[19] However, in the absence of two artificial added water molecules, the $^3$MLCT state originated from metal center to the bpy ligands was degenerated to lower than the dark state in both gas phase and water solution. Still this research was only based on one complex, and it was hard to find underlying principles of the Ru (II) polypyridine complexes' luminescence properties.

In order to fully understand the luminescence mechanisms of Ru(II) complexes, two Ru(II) polypyridine complexes ($[Ru(phen)_2dppzi]^{2+}$ (**2**) and $[Ru(phen)_2dppz\text{-}idzo]^{2+}$ (**3**); dppzi = dipyrido[3,2-a:2',3'-c]phenazine-10,11-imidazole, dppz-idzo = dipyrido-[3,2-a:2',3'-c]phenazine- imidazolone, **Scheme 1**) based on structure modification on the dppz ligand were synthetized and characterized in our laboratory.[20, 21] We have modified the main ligand of $[Ru(phen)_2dppz]^{2+}$ (**1**) and obtained two similar structured complexes, however, their luminescence properties underwent tremendous changes. For instance, by attaching an imidazole ring to the dppz ligand, complex **2** had an enlarged the π-extended planar, but in the presence of DNA or in aprotic solvent, its luminescence intensity had no significantly growth compared to $[Ru(phen)_2dppz]^{2+}$ (**1**).

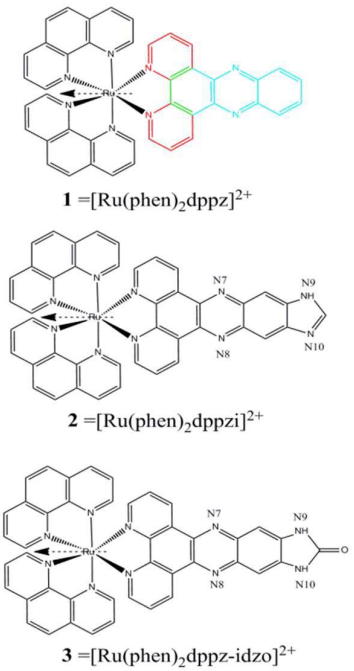


**Scheme 1** Chemical structures of $[Ru(phen)_2dppz]^{2+}$ (**1**), $[Ru(phen)_2dppzi]^{2+}$ (**2**), and $[Ru(phen)_2dppz\text{-}idzo]^{2+}$ (**3**). The red fragment was the bipyridine (bpy) part of the dppz ligand, the turquoise was the phenazine (phz) part, and the green was owned by both fragments. The arrows showed the calculated dipole moment direction.

To demystify the different luminescence mechanisms of these three complexes, theoretical calculations methods using TDDFT with natural transition orbitals (NTO) analysis, were applied to the titled complexes. By optimizing the triplet states structures of the complexes, we found that the complexes might emit red light through non-Kasha way. In other words, a steady triplet excited state ($^3$MLCT, refer in particular to "triplet transition of metal to coligands phenanthroline"), which was not the lowest triplet excited state ($T_1$), was calculated to be responsible for the emissive behaviour for all the three complexes. We also found that the luminescence properties of the complexes were likely related to their singlet vertical transitions in both gas phase and water. Thus, to elucidate the luminescence mechanism of the complexes, for the first time, we took their singlet excited transitions into account. By calculating the spin-orbital coupling (SOC) integral between the lowest singlet excited state, and both "bright state" and "dark state", we were able to explain the non-Kasha behaviour of the complexes. Furthermore, luminescence intensity change of the complexes in different circumstance was also interpreted by combining the SOC integral and radiative rate constants ($k_r$) of both "bright state" and "dark state".

## Experimental

### Materials

All chemicals were purchased from the manufacturer at analytically purity, and used without further purification. The DNA oligomer 5'-AGGGTTAGGGTTAGGGTTAGGG-3' was purchased from *Sangon (Shanghai, China)*. The concentrations of these oligomer samples were determined by measuring the absorbance at 260 nm. Single-strand extinction coefficients were calculated from mononucleotide data using a nearest-neighbor approximation. Detailed procedures for the synthesis of $[Ru(phen)_2(dppz)]^{2+}$ (**1**), $[Ru(phen)_2(dppzi)]^{2+}$ (**2**) and $[Ru(phen)_2(dppz\text{-}idzo)]^{2+}$ (**3**) could be found in Hartshorn et al[6], Shi[20] and Yao et al[21], respectively.

### Luminescence research

Luminescence spectra studies were carried out on a Hitachi F-7000 Fluorescence Spectrophotometer at room temperature. The concentration of the complexes were fixed at 5.0 μM and the luminescence was measured in the absence or presence of 2.5 μM human telomere G-quadruplex DNA, which serve as "light switches" for the complexes. The excitation wavelength was 460 nm and emission spectra were recorded in the range of 500-800 nm. The luminescence life time data of complex **1** and **3** were collected on a PTI QM/TM/IM Time-resolved Fluorescence Spectro-fluorometer (USA/CAN photon technology international Int.) at room temperature. Utilizing the picosecond pulses the time delay spectra of complex-acetonitrile solutions with 440 nm as excitation were detected at an emission wavelength of 610 nm for lifetime measurements with an emission polarizer and depolarizer.

### Computational Details

First, the geometry optimization of the titled complexes were performed for the singlet ground state using density functional theory (DFT) with Becke's three parameter hybrid functional with the Lee-Yang-Parr correlation functional (B3LYP) by Gaussian 09 (Rev: D.01).[22-24] A valence triple-ξ basis with polarization basis (6-311G**) was used for carbon, oxygen, nitrogen and hydrogen atoms. The basis set we used

has increased flexibility in the valence region relative to the 6-31G basis because it used three functions to represent each valence atomic orbital.[25] The ruthenium atom was represented with SDD (Stuttgart-Dresden ECP and D-basis set) basis set, which was the combination of the Stuttgart-Dresden basis set designed for a RECP (relativistic effective core potential) on core electrons with the Huzinaga-Dunning double-ξ basis set on valence electrons[26, 2726, 27 27, 28] Geometry optimizations for the complexes were carried out in gas phase and confirmed to be minima on their potential energy surfaces by calculation of their vibrational frequencies. Geometry optimizations were also performed in solution using water as solvent with the polarizable continuum model (PCM) and employing the same functional and basis set.

The luminescence properties were closely related to the stability of excited states of the complexes. Thus, the ten lowest singlet and triplet vertical transitions excited from the ground state ($S_0$) were calculated via TDDFT using the B3LYP functional at 6-311G**/SDD level. NTO analysis was carried out to resolve the compositions in the vertical excitations. The NTOs provided a much more compact description of "what was excited to where". Structure optimization of two triplet excited states of each complex, including the lowest excited state ($^3$LLCT, ligand to ligand charge transfer, the ligand referred to the π-extended ligand) and the lowest $^3$MLCT state, were carried out, which yielded the energy difference between the triplet excited states at their optimized geometry and the closed-shell ground state at the same geometry in the gas phase. This approach was a simple but reliable way to determine emission energies. These calculations were also performed in solution using water as solvent with the PCM, and employing the same functional and basis set as in the optimizations.

We then performed one-component zeroth order regular approximation (ZORA) TDDFT calculation, which included SOC perturbatively, with the Amsterdam Density Functional package (ADF 2014.07), [28-30] using the B3LYP functional with a Slater type DZP (double zeta plus polarization) basis for carbon, oxygen, nitrogen and hydrogen atoms and TZP (triple zeta plus polarization) basis for ruthenium atom. It was reported that the radiative rates using the perturbative spin−orbit approach gave results to within 15% of the full relativistic treatment. The relativistic effect, which was known to have a drastic influence on the molecular orbital alignment of transition metal (TM) complexes, was included by applying ZORA to the full relativistic effect treated in Dirac equation in order to properly account for the electronic structure in TM complexes. Environmental effects were also included via COSMO continuum solvation using water parameters while a range of media were used in available experimental data.

#### Calculation of spin-orbit coupling (SOC) integrals

SOC split the all the triplet states into three sublevels that are separated in energy in the absence of an applied field. This splitting was referred as the zero-field splitting. The phosphorescence radiative decay rate constants $k_r$ from one of the three substates $i$ ($i$ =1, 2, 3) of the certain triplet excited state $T_m$ to the ground state were expressed as[31-33]

$$k_r^i = \frac{1}{\tau_i} = \frac{4}{3t_0}\alpha_0^3(\Delta E_{S-T})^3 \sum_{j\in\{x,y,z\}}\left|M_j^i\right|^2 \quad \textbf{Eq1}$$

with $t_0 = (4\pi\varepsilon_0)^2\hbar^3/m_e e^4$ and $\alpha_0$ was the fine structure constant. $\Delta E_{S-T}$ was the transition energy, and $M_j^i$ was the $j$-axis projection of the electric dipole transition moment between the ground state and the $i^{th}$-substate of the triplet state. For the three substate of $T_m$ were almost equally populated in the high temperature limit, hence phosphorescence rates were calculated according,

$$k_r = \frac{1}{3}\sum_{i=1}^{3} k_r^i \quad \textbf{Eq2}$$

According to the Strickler–Berg relationship, in a medium, it was necessary to correct the calculated radiative rate $k_r$ multiply the square of the refractive index $n$ of the medium ($n_{water}$ = 1.333).[34]

The decay rate due to intersystem crossing between $S_n$ and $T_m$ was expressed by Fermi Golden Rule[32, 35-37]

$$k_{ISC}^{nm} = \frac{2\pi}{\hbar}\left\langle S_n\left|\hat{H}_{SO}\right|T_m\right\rangle^2 \times FCWD \quad \textbf{Eq3}$$

where $\left\langle S_n\left|\hat{H}_{SO}\right|T_m\right\rangle$ was the spin-orbit coupling (SOC) integral between the pure spin states $S_n$ and $T_m$, and FCWD was the Franck–Condon weighted density of states. Here, it was assumed that the FCWDs of the three complexes are of the comparable magnitude, where FCWD was proportional to the term exp[-($\Delta E_{ST}$/4$\lambda k_B T$)$^2$]. $\Delta E_{ST}$ was the energy gap between $S_n$ and $T_m$, while $\lambda$ was the Marcus reorganization energy, thus the main difference in FCWD might lie in $\Delta E_{ST}$, the FCWD increases as $\Delta E_{ST}$ decreases. For the ISC rate constant was proportional to the square of the SOC integral, while one triplet excited state was split into three sublevels, $T_x$, $T_y$ and $T_z$, which should be all taken into account. SOC integral was obtained by the equation below.[35]

$$\langle S_n|H_{SO}|T_m\rangle = \left\{\sum_{\alpha\in\{x,y,z\}}(Re^2\langle S_n|H_{SO}|T_{m,\alpha}\rangle + Im^2\langle S_n|H_{SO}|T_{m,\alpha}\rangle)\right\}^{1/2} \quad \textbf{Eq4}$$

where Re represents the real part of the SO matrix and Im represents the SO matrix imaginary part.

## Results and discussion

#### Experimental Luminescence and Life Time Study

The luminescence spectra of the three complexes (5.0 μM) in aqueous solution and in the presence of human telomere G-quadruplex DNA (2.5 μM) were investigated and the results were depicted in **Fig. 1A**. Dissolved in water (the enlarged graph on top right of **Fig. 1A**), complex **1** (black curve) was nearly nonluminous, while complex **2** and **3** (green and blue curve, respectively) were found weakly emissive at around 610 nm. When the G-quadruplex DNA was added to the solutions, the luminescence intensity of complex **1** and **3** (red and orange curve) exhibited hundredfold of enhancements, while complex **2** (pink curve) only grew about twofold. More interestingly, the spectra also showed that complex **2** possessed a new emission around 650 nm. The luminescence spectra of the complexes were also detected in acetonitrile (**Fig. S1A**), and their intensity difference was displayed in **Fig. 1B**. The emission energy maximum of all three complexes hardly changed when their medium changed,

**Table 1** Selected calculated bond lengths (nm), dihedral angels (deg), and change of dipole moment of the free molecules dissolved in water. Using the DFT-B3LYP at the SDD/6-311G** level.

| Complex | | Ru-$N_m$/nm[a] | Ru-$N_{co}$/nm | $A_m$/deg[b] | $A_{co}$/deg | Dihedral Angle/deg[c] | Dipole moment/D[d] |
|---|---|---|---|---|---|---|---|
| | | | | | | N7-N8-N9-N10 | |
| **1 in gas phase** | | 0.2111 | 0.2111 | 78.5 | 78.7 | | 5.87 |
| **2 in gas phase** | | 0.2111 | 0.2111 | 78.5 | 78.7 | 179.8 | 7.80 |
| **3 in gas phase** | | 0.2111 | 0.2111 | 78.5 | 78.7 | 179.7 | 11.41 |
| **1 in water** | cal | 0.2105 | 0.2107 | 78.5 | 78.8 | | 10.01 |
| | exp | 0.2065 | 0.2050 | 78.0 | 78.3 | | |
| **2 in water** | | 0.2105 | 0.2107 | 78.5 | 78.8 | 180.0 | 12.93 |
| **3 in water** | | 0.2106 | 0.2107 | 78.5 | 78.8 | 179.8 | 17.55 |

[a] Ru-$N_m$ was the mean coordination bond length (nm) between Ru and N atoms of the π-extended ligand, and Ru-$N_{co}$ expresses that between Ru and N atoms of the coligand (phen). [b] $A_m$ expresses the mean coordination bond angle (deg) between central Ru and two N atoms of the π-extended ligand, and $A_{co}$ expresses that of the coligand. [c] (N7-N8-N9-N10) was the dihedral angle (deg) between the four uncoordinated nitrogen atoms (**Scheme 1**). [d] dipole moment represented the calculated dipole moment values (D = debye).

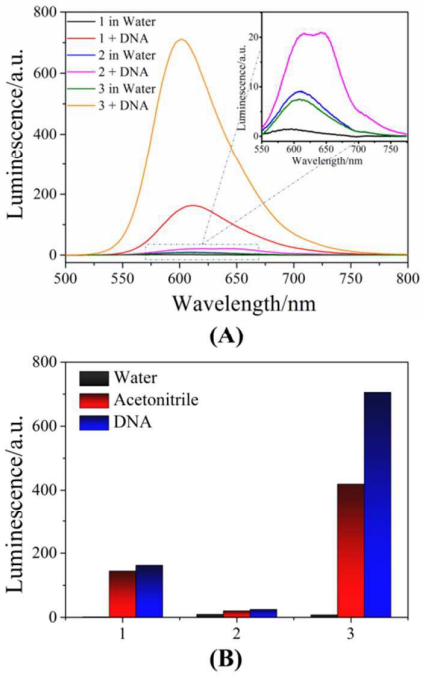


**Fig. 1** (**A**) Emission spectra ($\lambda_{ex}$ = 440 nm) of 5.0 μM $[Ru(phen)_2dppz]^{2+}$ (**1**), $[Ru(phen)_2dppzi]^{2+}$ (**2**), and $[Ru(phen)_2dppz\text{-}idzo]^{2+}$ (**3**) in the absence and presence of G-quadruplex DNA (2.5 μM, in 10 mM tris-HCl, 100 mM KCl, pH 7.0); (**B**) Luminescence intensity comparison column ($\lambda_{em}$ = 610 nm) of the three complexes in water, acetonitrile and interacting with DNAs.

which indicated the complexes might have a simple charge-transfer excited state. Since complex **1** and **3** were also strong emissive in acetonitrile, the luminescence life time data at 610 nm were measured at room temperature (**Fig. S1B**). The results were well fitted by one-exponential decay function with τ (**1**) = 147 ns and τ (**3**) = 154 ns.

### Ground State Structures Optimization

To gain further understanding on internal mechanisms of the luminescence and water-quenching properties of these three complexes, computational investigations were carried out. As displayed in **Table 1**, the predicted bond lengths (Ru-N) and angles of optimized complex **1** in water were close to the experimental values,[38] which indicated that the calculation results obtained were precise and reliable. According to the dihedral angles among the uncoordinated nitrogen atoms, the modified heterocyclic rings were kept in the same plane with dppz ligand. The complexes' frameworks shrink a little when water was imported to the calculation, implied by their shorter bonds length between Ru (II) and nitrogen atom in water than that in gas phase. The results in **Table 1** also suggested that dipole moments increased from **1** to **3** and solvent changed from gas to water**.** As shown in **Scheme 1**, the direction of the complexes' dipole moment was all pointed to the opposite direction of main ligands. According to **Eq5**, the value of dipole moment ($\mu$) was the arithmetic product of charges ($q$) and distance ($l$) between the positive and negative charges, while its direction was from positive charge center pointed to negative center.

$$\mu = q \cdot l \quad \textbf{Eq5}$$

However, the electrons were transferred from the π-extended ligand to Ru (II) center and phenanthroline ligands (**Table S1**) as the conjugate plance enlarged from **1** to **3**. Thus, we believed that the successive increase of dipole moment was caused by the growth of the π-extended conjugate plance, which enlarged $l$ in **Eq5**. Also, the dipole moments of the complexes were much larger in water solution than in gas phase, for the electrons were transferred from the two phenanthroline coligands and ruthenium (II) to the π-extended ligands (**Table S1**).

### Vertical Transitions Studies for the Complexes

TDDFT calculations were carried out to investigate the vertical transitions process.[39] Herein, the ground state of the complexes was singlet, which meant the spin-allowed excitations for the complexes were singlet transitions. However, for these three complexes, the lowest excited state were triplet, which could not be directly populated by light absorption, but could be obtained from the deactivation of upper singlet or triplet excited states. For this reason, at least three states (e.g., ground state singlet and the lowest excited singlet and triplet) were involved in a photochemical process.[2] Consequently, in order to gain comprehensive understanding of the complexes, ten lowest triplet vertically transitions of the complexes were also obtained using the same methods.

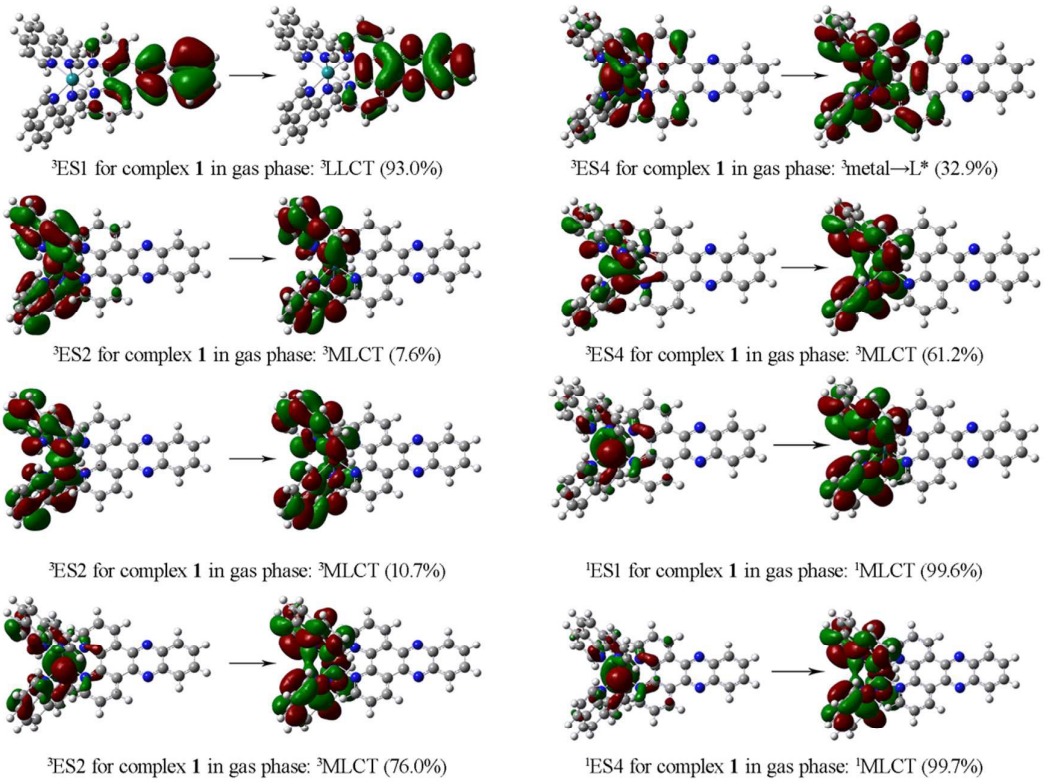


**Fig. 2** Selected NTO analysis results of the singlet and triplet vertical transitions of complex **1** in gas phase, corresponding to **Table 2**. $^3$ES1 was a $^3$LLCT transition; $^3$ES2 was composed of three $^3$MLCT transitions; $^3$ES4 was consisted of 32.9 percent of $^3$Metal→(phen* + bpy*) and 61.2 percent of $^3$MLCT transitions; the first two singlet transitions were both classified as $^1$MLCT.

The TDDFT results (table 2 and Fig. 2) showed that the first seven vertical transitions of complex **1** in gas phase were triplet excitations. The NTO results indicated that the lowest excitation ($^3$ES1) of complex **1** was clearly a $^3$LLCT state (93.0%). $^3$ES2 and $^3$ES3 were two $^3$MLCTs, which originated from *d* orbitals of Ru (II) to anti π orbitals of phen. And these two $^3$MLCTs excited states were similar to the lowest triplet state of $[Ru(phen)_3]^{2+}$, whose light emission was relatively insensitive to the presence of water. $^3$ES4-$^3$ES7 were the combinations of $^3$MLCTs and $^3$metal→bpy* (metal→bpy* meant the transition was inspired from metal to bpy part of the dppz ligand). First two singlet transitions of **1** in gas phase, were calculated to be $^1$MLCTs (**Fig. 2**).

The first three triplet transitions of complex **2** (**Table S2**) were similar to that of **1**, one $^3$LLCT followed by two $^3$MLCTs. However, the first singlet transition ($^1$ES1) of complex **2** appeared much earlier and was categorized as $^1$LLCT, which was also different from $^1$ES1 of complex **1**. $^3$ES6, $^1$ES4 and $^1$ES5 of **2** belonged to transitions from Ru (II) to phen* ($^3$MLCT or $^1$MLCT). For complex **3** (**Table S3**), the condition for both singlet and triplet transitions were similar to complex **1**, except that the first two triplet transitions of **3** were $^3$LLCTs, while the $^3$MLCT of **3** came as $^3$ES3 and $^3$ES4.

In water, the first triplet state of the titled complexes was mainly consisted of $^3$LLCT (**Table S4-S6**). Above the $^3$ES1 state, at least one $^3$MLCT state could be found for all complexes ($^3$ES3 for complex **1** and **2**, $^3$ES2 for **3**). The lowest singlet excited state ($^1$ES1) for all three complexes was summarized as $^1$metal→π*. For complex **1** (**Table S4**), above the $^1$metal→π* state, about 0.15 to 0.17 eV higher, a set of $^1$metal→L* excitations was followed. However, no transition that only consisted of $^1$MLCT was found for **1**. For complex **2** and **3**, their second singlet excited state was calculated to be $^1$MLCT.

The results of complex **1** here were similar to the results in previous reports.[18, 19, 41, 42] For instance, the optimized ground structure of **1** in water had same bond length as reported by Li et al, and the bond angles here was closer to the experimental data. [41] The highest occupied molecular orbital (HOMO) and the lowest unoccupied molecular orbital (LUMO) in water and gas phase had similar composition as described by Fantacci et al, [42] besides, the energy gap between HOMO and LUMO was very close to the data we have obtained (**Fig. S2**). Furthermore, the TDDFT results of the triplet transitions of **1**, was consistent with the results obtained by Enrique et al and Pourtois et al.[18,19] However, for the TD-DFT calculation in acetonitrile resulted similarly water solution, which indicated that the emission mechanism of the complexes between DNA and aprotic solvents might have different paths. [42]

The structures of the complexes were similar to each other, but their luminescence properties were quite different. Based on the data we have collected by now, it was noticeable that

**Table 2** TDDFT calculated energies, oscillator strengths (*f*), and natural transition orbital analysis results of the ten lowest-energy singlet and triplet excited states of $[Ru(phen)_2dppz]^{2+}$ (**1**) in gas phase.

| Excited State | $\lambda_{abs}$/nm(eV) | *f* | NTO Results |
|---|---|---|---|
| $^3$**ES1** | 566.09(2.19) | 0.0000 | $^3$LLCT (93.0%)[a] |
| $^3$**ES2** | 510.08(2.43) | 0.0000 | $^3$MLCT (94.4%)[b] |
| $^3$**ES3** | 505.16(2.45) | 0.0000 | $^3$MLCT (94.1%) |
| $^3$**ES4** | 497.14(2.49) | 0.0000 | $^3$metal→L* (32.9%)[c] |
| | | | $^3$MLCT (61.2%) |
| $^3$**ES5** | 482.62(2.57) | 0.0000 | $^3$metal→bpy*(12.4%)[d] |
| | | | $^3$MLCT(85.5%) |
| $^3$**ES6** | 477.80(2.59) | 0.0000 | $^3$MLCT (5.9%) |
| | | | $^3$metal→L* (7.9%) |
| | | | $^3$metal→bpy*(81.5%) |
| $^3$**ES7** | 468.50(2.65) | 0.0000 | $^3$MLCT (25.0%) |
| | | | $^3$metal→bpy*(70.2%) |
| $^1$**ES1** | 468.19(2.65) | 0.0006 | $^1$MLCT (99.6%)[e] |
| $^1$**ES2** | 466.74(2.66) | 0.0001 | $^1$MLCT (99.7%) |
| $^3$**ES8** | 459.19(2.70) | 0.0000 | |
| $^3$**ES9** | 455.05(2.72) | 0.0000 | |
| $^3$**ES10** | 452.88(2.74) | 0.0000 | |
| $^1$**ES3** | 451.28(2.75) | 0.0001 | $^1$metal→bpy*(99.3%)[f] |
| $^1$**ES4** | 441.94(2.80) | 0.0015 | |
| $^1$**ES5** | 439.67(2.82) | 0.0101 | |
| $^1$**ES6** | 427.92(2.90) | 0.0423 | |
| $^1$**ES7** | 422.59(2.93) | 0.0228 | |
| $^1$**ES8** | 419.97(2.95) | 0.0358 | |
| $^1$**ES9** | 414.36(2.99) | 0.1689 | |
| $^1$**ES10** | 408.39(3.04) | 0.0139 | |

[a] $^3$dppz→dppz* was considered as $^3$LLCT transition in the context; [b] $^3$MLCT was referring to triplet metal to coligands charge transfer in the context; [c] $^3$metal→L* represented for $^3$metal→(phen* + bpy*), which contained both coligand and main ligand parts; [d] $^3$Metal→bpy* was the triplet transition from metal to bpy part of the DPPZ ligand; [e] $^1$MLCT was singlet transition referring singlet metal to coligands charge transfer in the context; [f] $^1$metal→bpy* was the singlet transition from metal to bpy part of the dppz ligand .

the luminescence properties of the complexes seemed like to be related to their singlet vertical excitations at certain level. When interacting with DNA molecules, complex **1** and **3** were strongly emissive and their singlet and triplet transitions in gas phase were analogical. However, complex **2** exhibited distinctive singlet vertical transitions in gas phase, while its luminescence in the presence of DNA was quite unique. The same situation was applied to the complexes dissolved in water. Complex **2** and **3** were weakly emissive in water, while complex **1** was non-emissive. Here, we found that the first several singlet vertical transitions of complex **2** and **3** in water were similar to each other, while the data of complex **1** was distinctive. Bearing this in our mind, we then optimized the excited states energies of the complexes using the calculations in gas phase to simulate "luminescence on" state, [19] and modelling the non-luminous situation through the calculations in water.

**Studies on the Optimized Triplet Excited States**

Energy optimizations on the frontier triplet excited states of the complexes were then carried out, for these states played essential roles in luminescence of the complexes. A "bright and dark state" theory has been proposed to elucidate the luminescence mechanisms.[16-19,43,44] According to Pourtois's research, the $^3$LLCT state achieved above were the dark states, while the bright state of $[Ru(bpy)_2dppz]^{2+}$ was with a ligand orbital similar in size to that associated with the $^3$MLCT state of $[Ru(bpy)_3]^{2+}$.[44] Here, the triplet metal to phenanthroline transition ($^3$MLCT) obtained by TDDFT calculation was treated as the "bright state", while the $^3$LLCT was taken as the "dark state" of the titled complexes. All three complexes shared an emission peak at around 610 nm, it was reasonable to presume that the excited state responsible for this emission should possess similar energy levels or similar transitions. In the present study, geometry optimization was carried out for both "dark state" and "bright state" of the titled complexes in gas phase and aqueous solution, which yielded more accurate energy differences between the optimized triplet excited states and the closed-shell ground state at the same geometry. The obtained energy differences and the singlet vertical transitions (first transition for each complex) which were closely related to the luminescence properties of the complexes were depicted in **Fig. 3** and **Fig. 4**, while the coordinate information was available in the supplementary.

In gas phase, or in the case of luminescence, the first two singlet excited states of complex **1** (**Fig. 3A** and **Table 2**) were $^1$MLCTs at around 2.65 eV. The singlet excited state was very unstable, which would deactivate through intersystem crossing to lower lying triplet excited states immediately. The $^3$LLCT of complex **1** lied at 1.47 eV above a saddle point of the ground state (**Fig. 3A**, second transition). For the bright state path of complex **1** (**Fig. 3A**, third transition), the optimized triplet geometry showed that the lowest state was $^3$MLCT, while the $^3$LLCT state was lifted 0.29 eV above it. Complex **3** (**Fig. 3C**) had lots of similarities compared to **1**. The first two singlet transitions of complex **3** in gas phase were classified as $^1$MLCTs (**Table S3**) at 2.62 eV. The optimized $^3$LLCT of **3** lied at 1.79 eV above its closed shell singlet structure. For the optimized $^3$MLCT state, the $^3$LLCT state was also raised up about 0.34 eV above the $^3$MLCT. However, the singlet transitions and the optimized $^3$MLCT state of complex **2** shared few similarities with **1** and **3**. For complex **2** in gas phase, the lowest singlet transition was calculated as $^1$LLCT at 2.45 eV, which was followed by two $^1\pi_{(dppzi)} \rightarrow \pi_{(dppzi + phen)}$* transitions. The $^1$ES4 and $^1$ES5 of complex **2** were classified as $^1$MLCT at 2.62 eV. The optimized $^3$LLCT of **2** had a much lower energy level than those of **1** and **3**, and also for the optimized $^3$MLCT state of **2**, the $^3$LLCT still lied below the $^3$MLCT state about 0.07 eV, which might be corresponding to the emission peak at 610 nm and 650 nm of complex **2**.

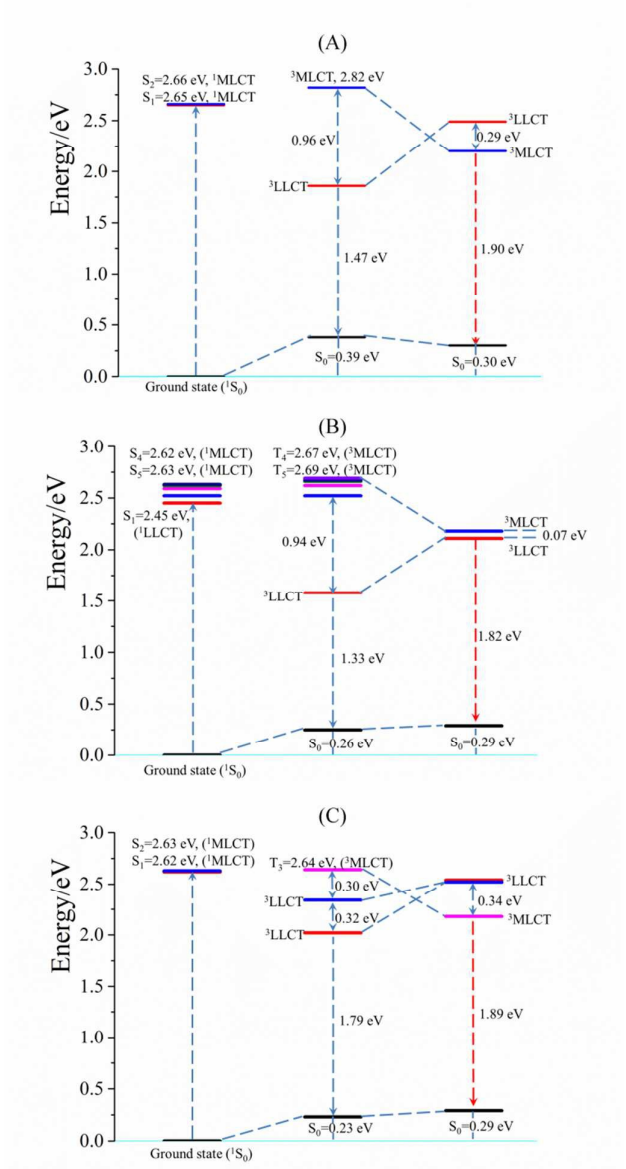


**Fig. 3** Calculated transition energy of complex **1** (A), **2** (B) and **3** (C) in gas phase. For each complex, the first transition was the excitation from ground state to their lowest singlet excited states; the second $^3$LLCT transition was the lowest triplet state for the three complexes, also referring as the dark state; the third one was the lowest $^3$MLCT transition of the three complexes, the lowest bright state of the complexes in gas phase.

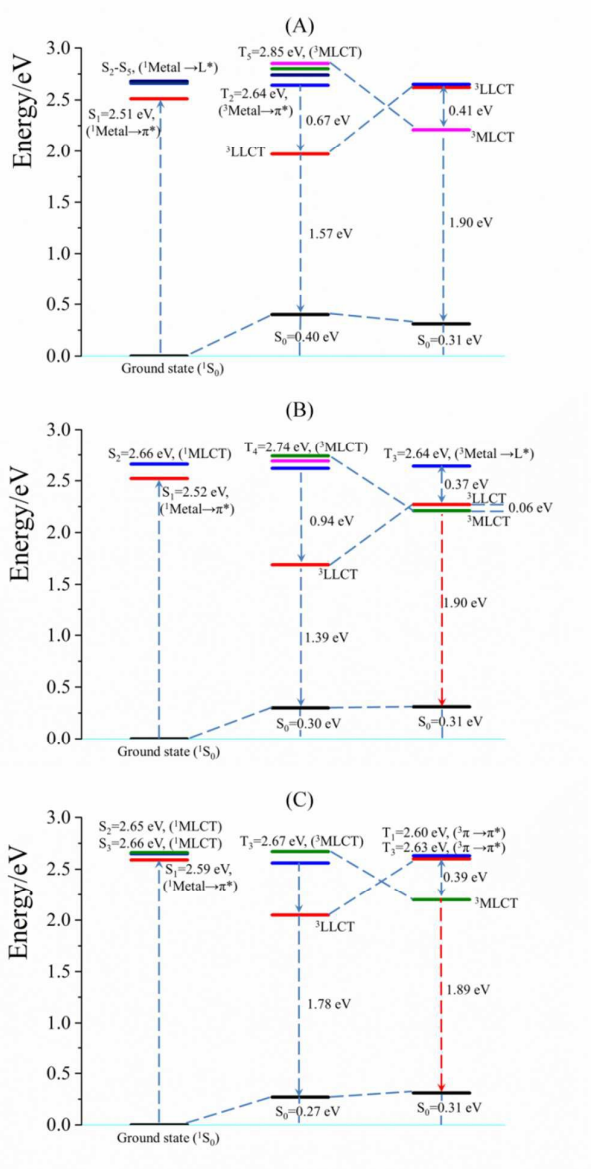


**Fig. 4** Calculated transition energy of complex **1** (A), **2** (B) and **3** (C) in water. For each complex, the first transition was the excitation from ground state to lowest singlet excited state; the second $^3$LLCT transition was the lowest triplet state for the three complexes; the third one was the lowest $^3$MLCT transition of the three complexes.

In water, the lowest triplet excited states or the "dark state" for all three complexes was classified as $^3$LLCT, which were similar to those in gas phase. For the optimized "bright state" in water (**Fig. 4**, third transition of each graph), complex **1** and **3** still had similar $^3$LLCT transition above the $^3$MLCT energy as in gas phase. However, for complex **2**, the original lower laid $^3$LLCT state in gas phase, was raised above the $^3$MLCT state about 0.06 eV, which might be the reason of the disappearance of the 650 nm emission. As for the singlet transitions, all three complexes had similar $^1$metal→π* transition as their $S_1$. However, for **2** and **3**, they both had at least one $^1$MLCT singlet transition ($^1$ES2 for **2**, $^1$ES2 and $^1$ES3 for **3**), while complex **1** had no such vertical excitation but the combination of $^1$MLCT and $^1$metal→dppz* with the $^1$MLCT percentage dropped from 83.9% to 42.5% (Table S4).

By employing energy optimizations on the excited states of the complexes, $^3$MLCT, was obtained as a steady triplet state during our simulation in both gas phase and water, with the energy of the $^3$MLCT calculated at 1.89-1.90 eV (**Fig. 3** and **Fig. 4**, third transition for each complex), which might be responsible for the 610 nm emission of the titled complexes. The energy levels of optimized $^3$LLCT states varied from 1.33 to 1.79 eV (**Fig. 3** and **Fig. 4**, second transition for each complex), which was quite unstable and changed in different circumstance. According to the vertical transitions results,

$^3$LLCT or the "dark state" was always the first triplet excited states of the complexes, while the "bright state" was the second or third excited state of the complexes, which demonstrated that dark state was always the lowest in energy.[17] Thus, the luminescence of the complexes in both gas phase and water might be a non-Karsh emissive behaviour. Nevertheless, both bright and dark states of the complexes were triplet excited states, as missioned above, they should be obtained through intersystem crossing (ISC) from the other excited states, mostly from the lowest singlet excited state $S_1$.[45]

**Spin-orbit coupling study**

According to the data we obtained above, we assumed that intersystem crossing between singlet excited state and triplet excited state might play an important role to the luminescence properties of the titled complexes. In organic system, El-Sayed rule is well-recognized and qualitatively resolved lot of phosphorescence of aromatic compounds. In general, for conjugated organic molecules, when a transition involves a change in orbital type or an orbital angular momentum change, such as $^1$n,π*→$^3$π,π* transition, the intersystem crossing could easily take place. However, for transition metal (TM) complexes, the "heavy metal effect" accelerates the ISC rate, for it significantly enlarged the SOC integral.[46] Rate constants of intersystem crossing are calculated by Fermi's golden rule (Eq 3), in which the SOC integral between singlet and triplet state ($\langle S_n|H_{SO}|T_m\rangle$) and the energy between them ($\Delta E_{ST}$) determine the overall rate of ISC.[34, 35] To simplify the discussion, we first evaluated the ISC channel from the lowest possible singlet excited state ($S_1$) to both dark state ($^3$LLCT) and bright state ($^3$MLCT) of the titled complexes. The energy gaps between $S_1$ and both states were obtained through TDDFT calculation at the $S_0$ geometries from Table 2 and Table S2-S6.

**Table 3** Theoretically calculated SOC integral (obtained at $S_0$ geometry) between $S_1$ and $^3$LLCT or $^3$MLCT as well as the energy between them ($\Delta E_{ST}$) in gas phase and water solution.

| | Gas phase | | | |
|---|---|---|---|---|
| **Comple x** | $\langle S_1\|H_{SO}\|^3\text{LLCT}\rangle$ ($cm^{-1}$) | $\Delta E_{ST}$ (eV) | $\langle S_1\|H_{SO}\|^3\text{MLCT}\rangle$ ($cm^{-1}$) | $\Delta E_{ST}$ (eV) |
| **1** | 0.29 | 0.46 | 77.0 | 0.22 |
| **2** | 0.16 | 0.63 | 1.31 | 0.04 |
| **3** | 3.15 | 0.40 | 109 | 0.21 |
| | **Water** | | | |
| **1** | 38.2 | 0.21 | 39.3 | 0.06 |
| **2** | 5.33 | 0.57 | 83.3 | 0.08 |
| **3** | 27.0 | 0.31 | 106 | 0.15 |

Table 3 listed the SOC integral ($\langle S_1|H_{SO}|^3\text{LLCT}\rangle$, $\langle S_1|H_{SO}|^3\text{MLCT}\rangle$) followed by the singlet–triplet energy gap ($\Delta E_{ST}$). In gas phase, the first singlet excited state of complex **1** and **3** was characterized as $^1$MLCT (Fig 3 and Table 2 and Table S3), while $S_1$ of complex **2** was $^1$LLCT transition. For all the three complexes in gas phase, the SOC integral from $S_1$ state to $^3$LLCT was quite small, and also the energy gap between those two states was larger than other ones; these all indicated that ISC rate between $S_1$ and $^3$LLCT state was small and undesirable. As for complex **1** and **3**, the SOC integral $\langle S_1|H_{SO}|^3\text{MLCT}\rangle$ was much larger than that of $\langle S_1|H_{SO}|^3\text{LLCT}\rangle$; at the same time, the energy gap between $S_1$ and $^3$MLCT was smaller; these two features would result very fast ISC, and might cause the non-Kasha emission of these two complexes. The SOC integral $\langle S_1|H_{SO}|^3\text{MLCT}\rangle$ of complex **2** was much smaller than the other two complexes, which made the ISC procedure of complex **2** slower than that of **1** and **3** and the luminescence intensity of **2** smaller. However, the SOC integral $\langle S_1|H_{SO}|^3\text{MLCT}\rangle$ of complex **2** was larger than the SOC integral $\langle S_1|H_{SO}|^3\text{LLCT}\rangle$, also the energy gap of the former SOC was much smaller than the later one, which meant the non-Kasha emission was still possible for complex **2**.

In aqueous solution, the lowest singlet excited state of all the three complexes was classified as $^1$metal→π*, which might greatly affect the SOC integral between $S_1$ and $^3$LLCT or $^3$MLCT. The SOC integral $\langle S_1|H_{SO}|^3\text{LLCT}\rangle$ in water of all three complexes was much larger than that in gas phase. Meanwhile, the energy gap between $S_1$ and $^3$LLCT was significantly dropped, which meant the ISC rate between $S_1$ and $^3$LLCT was much faster than that in gas phase. For complex **1**, the SOC integral $\langle S_1|H_{SO}|^3\text{MLCT}\rangle$ reduced to 39.3 $cm^{-1}$, which was close to the SOC integral between $S_1$ and the $^3$LLCT state; this made it difficult for complex **1** to have an efficient ISC to the "bright state" and violate the Kasha rule. Both SOC integral $\langle S_1|H_{SO}|^3\text{MLCT}\rangle$ of complex **2** and **3** were much larger than that of the $\langle S_1|H_{SO}|^3\text{MLCT}\rangle$, which meant the ISC to the "bright state" of **2** and **3** was still very fast, they might be emissive in water.

**Table 4** The sum of the SOC integral between $S_i$ ($i$=1-6) and $^3$LLCT or $^3$MLCT in gas phase and water solution.

| | Gas phase | |
|---|---|---|
| **Complex** | $\Sigma\langle S_i\|H_{SO}\|^3\text{LLCT}\rangle$ ($cm^{-1}$) | $\Sigma\langle S_i\|H_{SO}\|^3\text{MLCT}\rangle$ ($cm^{-1}$) |
| **1** | 54.5 | 668 |
| **2** | 2.44 | 222 |
| **3** | 17.0 | 443 |
| | **Water** | |
| **1** | 440 | 392 |
| **2** | 39.4 | 329 |
| **3** | 176 | 326 |

For ISC from $S_1$ to both $^3$LLCT and $^3$MLCT might not be the most favourable ISC channel, we then calculated the SOC integral from $S_1$ to $S_6$ and summed them up (Table 4), which could deliver more insights into the overall ISC rate of the complexes. In gas phase, it seemed like that the singlet excited states intended to ISC to $^3$MLCT states than to $^3$LLCTs, for all the sum of SOC integral to $^3$MLCT was hundred times larger than that of $^3$LLCT. Within water solution, the sum of the SOC integral to $^3$LLCT state increased about ten times, which made it much easier for the singlet states to ISC to $^3$LLCT states. The SOC integral to $^3$MLCT state of complex **1** and **3** showed significant decrease, which might cause the luminescence dropping for them in water. The results we obtained here were similar to the $S_1$ SOC integral, which again indicated that the ISC rate to "bright and dark states" was an important

factor that dominating the luminescence properties of $[Ru(phen)_2dppz]^{2+}$ liked complexes.

The luminescence intensity of the complexes was not only associated with the ISC rate, but also related to the intrinsic luminescence radiative rate constants ($k_r$) and non-radiative rate constants ($k_{nr}$). The quantum yield ($\phi_r$) of the emission:

$$\phi_r = \frac{k_r}{k_r + k_{nr}} \quad \textbf{Eq 6}$$

for Ru (II) complexes, at room temperature, the temperature-independent non-radiative rate constants $k_{nr}$ followed the energy gap law (rates of non-radiative decay increase as the energy gap between ground and excited states decreases). [32] Here, the $^3$MLCT state of the complexes was the emissive state. The energy of $^3$MLCT only changed about 0.01-0.02 eV when the complexes moved from gas phase to water solution, which indicated that the $k_{nr}$ $^3$MLCT hardly changed and could be treated as a constant. The $^3$LLCT state of Ru (II) complexes was reported to have a non-radiative decay rate constant of the same order as the deactivation rate constant of $^3$MLCT states.[17] Since radiative decay from $^3$LLCT was very slow, the deactivation path of the $^3$LLCT state was mostly non-radiative.[18]

Chou et al reported that the luminescence intensity of TM complexes was roughly linearly with the theoretically evaluated $\langle S_n|H_{SO}|T_m\rangle^2 \cdot k_r$.[35] In the present study, the luminescence intensity of the titled complexes was likely proportional to the ratio between the "bright state's" and "dark state's" ISC rate constant, and also proportional to the ratio between $k_r$ ($^3$MLCT) and $k_{nr}$ ($^3$LLCT). As mentioned above, the non-radiative decay rate constant of the same order as the deactivation rate constant of $^3$MLCT states,[17] thus, we were able to evaluate the luminescence intensity of the complexes through the ratio of SOC integrals between $^3$MLCT and $^3$LLCT (i.e.$\{(\Sigma\langle S_i|H_{SO}|^3MLCT\rangle)^2\}/\{(\Sigma\langle S_i|H_{SO}|^3LLCT\rangle)^2\}$, $i$=1-6).

In gas phase or mixed with DNA, complex **1** and **3** showed strong emissions and the intensity of **3** was about four times larger than **1**. In table S7, the SOC ratio ($\{(\Sigma\langle S_i|H_{SO}|^3MLCT\rangle)^2\}/\{(\Sigma\langle S_i|H_{SO}|^3LLCT\rangle)^2\}$, $i$ =1-6) of complex **3** was also about four times larger than that of **1**. For complex **2**, though it had a very large SOC ratio, the optimized $^3$MLCT state could not bypass the lower lying $^3$LLCT state (Fig. 4B), which might greatly affect its luminescence intensity. In water, luminescence of **1** and **3** was quenched, because of the $^3$LLCT SOC integrals ($\Sigma\langle S_i|H_{SO}|^3LLCT\rangle$ ($i$=1-6)) were dramatically increasing, while the $^3$MLCT involved SOC integrals were dropping. For complex **1**, the $^3$LLCT SOC integral was larger than the $^3$MLCT SOC integral, which caused a completely quenched of the luminescence. For complex **2** and **3**, their "bright states SOC" overcame the "dark state SOC" and exhibited weak luminescence in water. Our results here could interpret the luminescence mechanism of the complexes interacting DNA, as for the luminescence in acetonitrile and other aprotic solvent, more studies need to be done.

## Conclusions

Luminescence mechanisms of ruthenium (II) poly-pyridine complexes had perplexed researchers for a long time. In order to provide a detailed insight into the nature of the luminescence properties of Ru (II) polypyridine complexes, we have systematic studied three complexes with similar structures and characteristic luminescence properties. Here, by optimizing the "bright state" and "dark state" structures, we have correlated theoretical emission energies with experimental values of the three complexes. We have also resolved the complexes' different luminescence intensity through calculating SOC integral and radiative rate constant.

In the compounds we investigated, the corresponding relationships between singlet vertical transitions and luminescence properties inspired us linking the "switch on" state to the gas phase simulation, and "switch off" state to the water solution calculations. The optimized triplet excited results indicated that the $^3$MLCT state might be the calculated "bright state", which seemed like to be responsible of the emissive characteristics of the three complexes, for it showed the best agreement of the computed emission energy with the experimental value and computed $k_r$ value was much larger than that of the $^3$LLCT state. The distinct luminescence of complex **2** was also interpreted by the optimization of the $^3$MLCT state, where the optimized $^3$MLCT was responsible for the emission at 610 nm and the $^3$LLCT state located 0.07 eV below the $^3$MLCT state was accountable for the emission at 650 nm. Finally, we calculated the SOC integral between $S_i$($i$ =1-6) and both "bright and dark state", combining with the radiative rate constant of "bright and dark state", which helped interpret the intersystem crossing between $S_i$ and "bright and dark state", and also brought up an semi-quantitative mechanism for the luminescence quenching by water.

## Acknowledgements

This work was supported by the National Natural Science Foundation of China (21472139, 31170776 and 81171646) and the Fundamental Research Funds for the Central Universities. We would like to acknowledge support from the developers at SCM (Dr. Fedor Goumans and his colleagues at *Fermitech*).

## Notes and references

1 J. P. Sauvage; J. P. Collin; J. C. Chambron; S. Guillerez; C. Coudret; V. Balzani; F. Barigelletti; L. De Cola; L. Flamigni, *Chem. Rev.,* 1994, **94**, 993-1019.
2 A. Juris; V. Balzani; F. Barigelletti; S. Campagna; P. Belser; A. von Zelewsky, *Coordin. Chem. Rev.,* 1988, **84**, 85-277.
3 L. Duan; F. Bozoglian; S. Mandal; B. Stewart; T. Privalov; A. Llobet; L. Sun, *Nat. Chem.,* 2012, **4**, 418-423.
4 M. K. Nazeeruddin; C. Klein; P. Liska; M. Grätzel, *Coordin. Chem. Rev.,* 2005, **249**, 1460-1467.
5 A. E. Friedman; J. C. Chambron; J. P. Sauvage; N. J. Turro; J. K. Barton, *J. Am. Chem. Soc.,* 1990, **112**, 4960-4962.
6 R. M. Hartshorn; J. K. Barton, *J. Am. Chem. Soc.,* 1992, **114**, 5919-5925.
7 R. E. Holmlin; E. D. A. Stemp; J. K. Barton, *Inorg. Chem.,* 1998, **37**, 29-34.

8 L. S. Ling; Z. K. He; G. W. Song; Y. E. Zeng; C. Wang; C. L. Bai; X. D. Chen; P. Shen, *Anal. Chim. Acta.,* 2001, **436**, 207-214.
9 J.-G. Liu; B.-H. Ye; H. Chao; Q.-X. Zhen; L.-N. Ji, *Chem. Lett.,* 1999, 1085-1086.
10 H. Song; J. T. Kaiser; J. K. Barton, *Nat. Chem.,* 2012, **4**, 615-20.
11 S. Shi; J. Zhao; X. Geng; T. Yao; H. Huang; T. Liu; L. Zheng; Z. Li; D. Yang; L. Ji, *Dalton Trans.,* 2010, **39**, 2490-3.
12 N. P. Cook; V. Torres; D. Jain; A. A. Marti, *J. Am. Chem. Soc.,* 2011, **133**, 11121-3.
13 N. P. Cook; M. Ozbil; C. Katsampes; R. Prabhakar; A. A. Marti, *J. Am. Chem. Soc.,* 2013, **135**, 10810-6.
14 K. I. Lira-De Leon; P. Garcia-Gutierrez; I. N. Serratos; M. Palomera-Cardenas; P. Figueroa-Corona Mdel; V. Campos-Pena; M. A. Meraz-Rios, *J. Alzheimers Dis.,* 2013, **35**, 319-34.
15 N. P. Cook; K. Kilpatrick; L. Segatori; A. A. Marti, *J. Am. Chem. Soc.,* 2012, **134**, 20776-82.
16 E. J. C. Olson; D. Hu; A. Hörmann; A. M. Jonkman; M. R. Arkin; E. D. A. Stemp; J. K. Barton; P. F. Barbara, *J. Am. Chem. Soc.,* 1997, **119**, 11458-11467.
17 M. K. Brennaman; J. H. Alstrum-Acevedo; C. N. Fleming; P. Jang; T. J. Meyer; J. M. Papanikolas, *J. Am. Chem. Soc.,* 2002, **124**, 15094-15098.
18 G. Pourtois; D. Beljonne; C. Moucheron; S. Schumm; A. Kirsch-De Mesmaeker; R. Lazzaroni; J. L. Bredas, *J. Am. Chem. Soc.,* 2004, **126**, 683-92.
19 E. R. Batista; R. L. Martin, *J. Phys. Chem. A,* 2005, **109**, 3128-33.
20 S. Shi; J. Zhao; X. Gao; C. Lv; L. Yang; J. Hao; H. Huang; J. Yao; W. Sun; T. Yao; L. Ji, *Dalton Trans.,* 2012, **41**, 5789-93.
21 J. L. Yao; X. Gao; W. Sun; X. Z. Fan; S. Shi; T. M. Yao, *Inorg. Chem.,* 2012, **51**, 12591-3.
22 C. Lee; W. Yang; R. G. Parr, *Phys. Rev. B,* 1988, **37**, 785-789.
23 A. D. Becke, *J. Chem. Phys.,* 1993, **98**, 5648.
24 M. J. Frisch; G. W. Trucks; H. B. Schlegel; G. E. Scuseria; M. A. Robb; J. R. Cheeseman; G. Scalmani; V. Barone; B. Mennucci; G. A. Petersson; H. Nakatsuji; M. Caricato; X. Li; H. P. Hratchian; A. F. Izmaylov; J. Bloino; G. Zheng; J. L. Sonnenberg; M. Hada; M. Ehara; K. Toyota; R. Fukuda; J. Hasegawa; M. Ishida; T. Nakajima; Y. Honda; O. Kitao; H. Nakai; T. Vreven; J. A. Montgomery Jr.; J. E. Peralta; F. Ogliaro; M. J. Bearpark; J. Heyd; E. N. Brothers; K. N. Kudin; V. N. Staroverov; R. Kobayashi; J. Normand; K. Raghavachari; A. P. Rendell; J. C. Burant; S. S. Iyengar; J. Tomasi; M. Cossi; N. Rega; N. J. Millam; M. Klene; J. E. Knox; J. B. Cross; V. Bakken; C. Adamo; J. Jaramillo; R. Gomperts; R. E. Stratmann; O. Yazyev; A. J. Austin; R. Cammi; C. Pomelli; J. W. Ochterski; R. L. Martin; K. Morokuma; V. G. Zakrzewski; G. A. Voth; P. Salvador; J. J. Dannenberg; S. Dapprich; A. D. Daniels; Ö. Farkas; J. B. Foresman; J. V. Ortiz; J. Cioslowski; D. J. Fox *Gaussian 09*, Gaussian, Inc.: Wallingford, CT, USA, 2009.
25 J.-P. Blaudeau; M. P. McGrath; L. A. Curtiss; L. Radom, *J. Chem. Phys.,* 1997, **107**, 5016.
26 M. A. Iron; A. C. Lucassen; H. Cohen; M. E. van der Boom; J. M. Martin, *J. Am. Chem. Soc.,* 2004, **126**, 11699-710.
27 A. V. Titov; N. S. Mosyagin, *Modern Methods and Algorithms of Quantum Chemistry*. John von Neumann Institute for Computing: Jülich, 2000; **1**.
28 ADF2014, SCM, Theoretical Chemistry, Vrije Universiteit, Amsterdam, Netherlands, http://www.scm.com.
29 G. te Velde; F. M. Bickelhaupt; E. J. Baerends; C. Fonseca Guerra; S. J. A. van Gisbergen; J. G. Snijders; T. Ziegler, *J. Comput. Chem.,* 2001, **22**, 931-967.
30 C. Fonseca Guerra; J. G. Snijders; G. te Velde; E. J. Baerends, *Theoretical Chemistry Accounts: Theory, Computation, and Modeling,* 1998, **99**, 391-403.
31 J. M. Younker; K. D. Dobbs, *J. Phys. Chem. C,* 2013, **117**, 25714-25723.
32 D. Escudero; D. Jacquemin, *Dalton Trans.,* 2015, **44**, 8346-55.
33 S. P. McGlynn; T. Azumi; M. Kinoshita, *Molecular Spectroscopy of the Triplet State*. Prentice Hall: Engelwood Cliffs, New Yersey, 1969.
34 K. Mori; T. P. Goumans; E. van Lenthe; F. Wang, *Phys. Chem. Chem. Phys.,* 2014, **16**, 14523-30.
35 E. Yu-Tzu Li; T.-Y. Jiang; Y. Chi; P.-T. Chou, *Phys. Chem. Chem. Phys.,* 2014, **16**, 26184-26192.
36 G. W. Robinson; R. P. Frosch, *J. Chem. Phys.,* 1963, **38**, 1187.
37 V. Lawetz; G. Orlandi; W. Siebrand, *J. Chem. Phys.,* 1972, **56**, 4058.
38 H. Niyazi; J. P. Hall; K. O'Sullivan; G. Winter; T. Sorensen; J. M. Kelly; C. J. Cardin, *Nat. Chem.,* 2012, **4**, 621-8.
39 E. Runge; E. K. U. Gross, *Phys. Rev. Lett.,* 1984, **52**, 997-1000.
40 R. L. Martin, *J. Chem. Phys.,* 2003, **118**, 4775.
41 J. Li; J.-C. Chen; L.-C. Xu; K.-C. Zheng; L.-N. Ji, *J. Organomet. Chem.,* 2007, **692**, 831-838.
42 S. Fantacci; F. De Angelis; A. Sgamellotti; N. Re, *Chem. Phys. Lett.,* 2004, **396**, 43-48.
43 X. H. Lu; S. Shi; J. L. Yao; X. Gao; H. L. Huang; T. M. Yao, *J. Inorg. Biochem.,* 2014, **140C**, 64-71.
44 M. K. Brennaman; T. J. Meyer; J. M. Papanikolas, *J. Phys. Chem. A,* 2004, **108**, 9938-9944.
45 L. Serrano-Andrés; M. Merchán, *J. Mol. Struc.: Theochem,* 2005, **729**, 99-108.
46 P. Klán; J. Wirz, *Photochemistry of Organic Compounds: From Concepts to Practice*. John Wiley & Sons Ltd: 2009; 25-71.

Graphic abstract

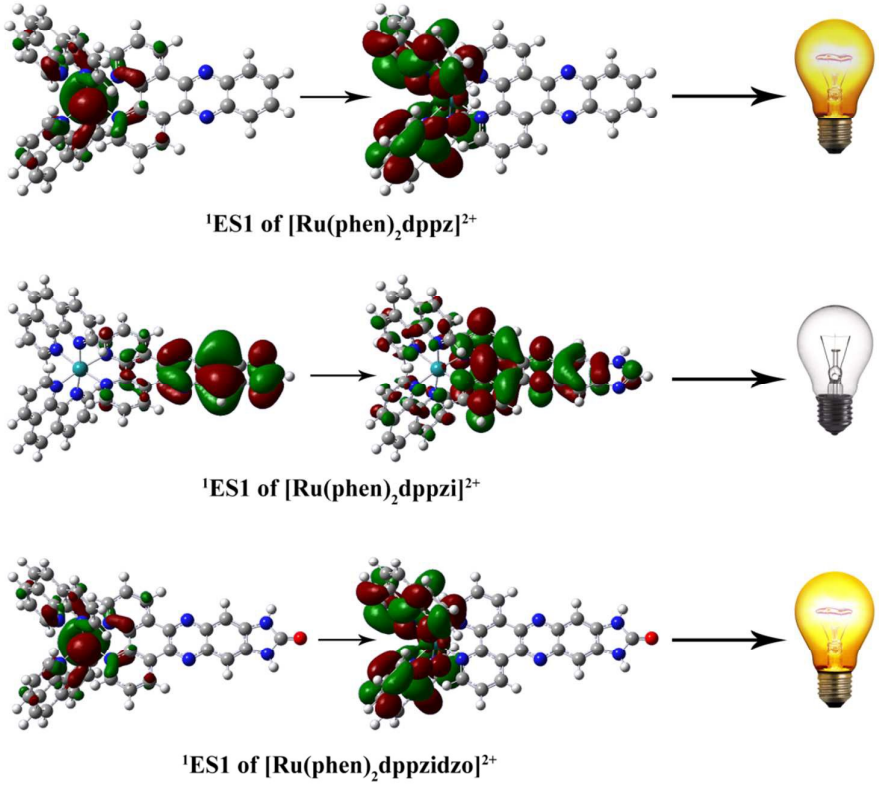


Lowest singlet transitions were found to be related to the intriguing luminescence properties of three different dppz-liked ruthenium (II) complexes through theoretical study.